AAPPS Bulletin

ORIGINAL ARTICLE

Open Access

Wavelength multicasting quantum clock synchronization network

Jiaao Li[1,2†], Hui Han[3,4†], Xiaopeng Huang[1,2], Bangying Tang[5], Kai Guo[6], Jinquan Huang[4,7], Siyu Xiong[4,8], Wanrong Yu[3], Zhaojian Zhang[2], Junbo Yang[2], Bo Liu[4*], Huan Chen[2*] and Zhenkun Lu[1*]

Abstract

Quantum clock synchronization (QCS) can measure out the high-precision clock difference among distant users, which breaks through the standard quantum limit by employing the properties of quantum entanglement. Currently, the wavelength division multiplexed QCS network has been demonstrated with a spontaneous parametric down-conversion entangled photon source. In this paper, we propose a more efficient QCS network scheme with the wavelength multicasting entangled photon source, which can decrease at least 25% of wavelength channel consumption under the identical network scale. Afterwards, a four node QCS network is demonstrated, where the wavelength multicasting entangled photon source is utilized with dual-pumped four-wave mixing silicon chip. The experimental results show that the measured time deviation is 3.4 ps with an average time of 640 s via the multiple fiber links of more than 10 km.

Keywords Wavelength multicasting, Silicon chip, Quantum clock synchronization network

1 Introduction

High-precision clock synchronization has been an indispensable technology in numerous fields such as navigation [1], geodesy [2], astronomy [3], long baseline interferometry [4, 5], and communication [6–9]. Quantum clock synchronization (QCS) can measure out the high-precision clock difference among distant users, which breaks through the standard quantum limit by employing the properties of quantum entanglement. Currently, the QCS schemes that have been successfully verified include two-way QCS [10–13], Hong-Ou-Mandel (HOM) interferometer-based QCS [14], and round-trip QCS [15, 16]. In 2023, Tang et al. proposed a QCS network scheme using wavelength division multiplexing (WDM) with a magnesium oxide-doped periodically poled lithium niobate (MgO: PPLN) crystal spontaneous parametric down-conversion (SPDC) entangled photon source, where the number of wavelength channels to be occupied is $2m$ for m users [15]. The pair of entangled wavelength channels generated by SPDC [17] can only provide clock measurements between a single user and

†Jiaao Li and Hui Han contributed equally to this work.

*Correspondence:
Bo Liu
liubo08@nudt.edu.cn
Huan Chen
chenhuan11@nudt.edu.cn
Zhenkun Lu
lzk06@sina.com
[1] College of Electronic Information, Guangxi University For Nationalities, Nanning 530006, China
[2] College of Science, National University of Defense Technology, Changsha 410073, China
[3] College of Computer, National University of Defense Technology, Changsha 410073, China
[4] College of Advanced Interdisciplinary Studies, National University of Defense Technology, Changsha 410073, China
[5] Strategic Assessments and Consultation Institute, Academy of Military Sciences, Beijing 100091, China
[6] Institute of Systems Engineering, Academy of Military Sciences, Beijing 100039, China
[7] School of Electronics and Communication Engineering, Shenzhen Campus of Sun Yat-sen University, Shenzhen 518107, China
[8] School of Mathematical Sciences, Sichuan Normal University, Chengdu 610068, China

the server, this scheme faces difficulties such as excessive wavelength channel consumption and complex cabling.

Four-wave mixing (FWM) can also be used to fabricate entangled photon sources, which can use multiple beams of pump light of different wavelengths to achieve wavelength multicasting [18, 19]. The wavelength channels of entangled photon pairs generated by the SPDC effect are one-to-one relationships, but the wavelength multicasting through the multi-pump FWM effect can establish the entanglement relationship between a signal photons wavelength channel and multiple idler photons wavelength channels. In addition, wavelength multicasting of FWM is similar to wavelength conversion, which can be used for networking through WDM [18, 20] and decreases the wavelength channel consumption and the cabling complexity when applied to quantum computing, quantum communication, QCS, etc. [15, 21–25].

In this paper, we propose a more efficient QCS network scheme with the wavelength multicasting entangled photon source, which can decrease at least 25% of wavelength channel consumption compared with the scheme proposed by Tang et al. [15] under the same network scale. Afterwards, the four node QCS network is demonstrated, where the wavelength multicasting entangled photon source utilize with dual-pumped FWM silicon chip. The demonstration lasted for 11.1 h. The fiber of 10 km connection is between Alice and Charlie server, and 25 km fiber connection is between Bob and server. The time deviation (TDEV) between the server and each user (Alice, Bob, and Charlie) at an average time of 640 s is 3.43 ps, 2.03 ps, and 2.44 ps, respectively. Furthermore, the wavelength multicasting QCS network provides the foundation for the construction of larger-scale QCS networks, which are anticipated to play a pivotal role in future quantum networks.

2 Wavelength multicasting entangled photon source

FWM is a nonlinear optical phenomenon that obeys the law of conservation of energy. In the phenomenon, two pump photons with wavelength λ_p and λ_q annihilate to generate a pair of signal and idler photons with wavelength λ_s and λ_i, that is $\lambda_p + \lambda_q = \lambda_s + \lambda_i$ [26–28]. FWM facilitates the energy conversion from one wavelength to another, known as the wavelength conversion [29], or to several wavelengths, known as the wavelength multicasting [30]. We utilize dual-pumped FWM to prepare a wavelength multicasting entangled photon source. As shown in Fig. 1, the pump photons (λ_p and λ_q) converted to signal photons (λ_s) and idler photons (λ_q^1, λ_q^2, and λ_q^3), under the action of degenerate and non-degenerate FWM. Once λ_s is selected as the wavelength channel of the signal photon, according to the law of energy conservation, there are three idler photon channels entangled with it, with wavelength of λ_i^1 ($\lambda_p + \lambda_p - \lambda_s$), λ_i^2 ($\lambda_p + \lambda_q - \lambda_s$), and λ_i^3 ($\lambda_q + \lambda_q - \lambda_s$), respectively. Multiple sets of wavelength multicasting entanglement can be chosen to build a QCS network according to the scale of the network. This method provides a scalable and adaptable architecture for the needs of multi-node networking. Furthermore, according to the calculation, the number of idler photon channels entangled with a signal photon

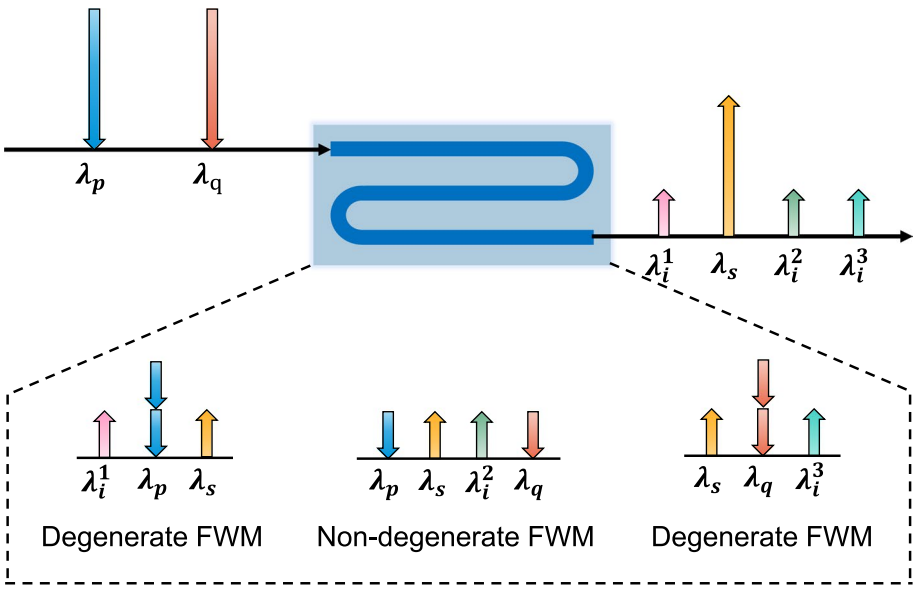

Fig. 1 Dual-pumped FWM wavelength multicasting entangled photon source. Under the action of degenerate and non-degenerate FWM, the pump photons (λ_p and λ_q) converted to signal photons (λ_s) and idler photons (λ_q^1, λ_q^2, and λ_q^3)

channel is $s + \binom{s}{2} = \frac{s(s+1)}{2}$, when the number of pump lights with different wavelengths is s.

3 QCS network scheme

Take the double-pump FWM as an example, the proposed wavelength multicasting round-trip QCS network scheme is shown in Fig. 2. The entangled photons generated by the wavelength multicasting entanglement photon source are demultiplexed into photons with wavelengths λ_i^j (idler) and λ_s^k (signal), $j \in [1, 3n], k \in [1, n], n \in N^*$ by a dense wavelength-division multiplexing (DWDM).

Here, we take the clock synchronization process between User_1 and the server as an example for a detailed explanation. The signal photons with the wavelength of λ_s^1 are separated from the DWDM and directly detected at the server. The idler photons with the wavelength of λ_i^1 are sent into the round-trip detection module (RTD_1), pass through optical circulate (OC) (from port 1 to port 2), and a section of optical fiber to reach the user photon detection module (UPD_1), and are transmitted to BS from port 3 of OC. The photons are divided into two parts by beam splitter (BS). One part is directly detected, and one part enters from port 1 of OC, exits from port 2, and returns to the RTD_1 of the server. The returned photons are transmitted from port 3 of OC and detected. The outputs of all detectors are connected to the time-to-digital converter (TDC) synchronized with their local clocks.

The entangled photon pairs produced by FWM are time-correlated [31–33]. The time difference between the signal-idler photon pairs measured at two space-time points (r_1, t_1) and (r_2, t_2) is given by the peak position of the second-order correlation function $G^{(2)}$, which is derived from the joint distribution [34, 35].

$$G^{(2)}(r_1, t_1, r_2, t_2) = \left\langle E^{(-)}(r_1, t_1) E^{(-)}(r_2, t_2) E^{(+)}(r_1, t_1) E^{(+)}(r_2, t_2) \right\rangle, \tag{1}$$

where $E^{(+)}$ and $E^{(-)}$ are the positive-frequency and negative-frequency part of the electric field operators at space-time point $(r_i, t_i), i = 1, 2$. The time when the signal photons are detected is recorded as t_1. The times at which the idler photons are detected by the UPD_1 and returning to the RTD_1 are recorded as t_1 and t_2, respectively. The

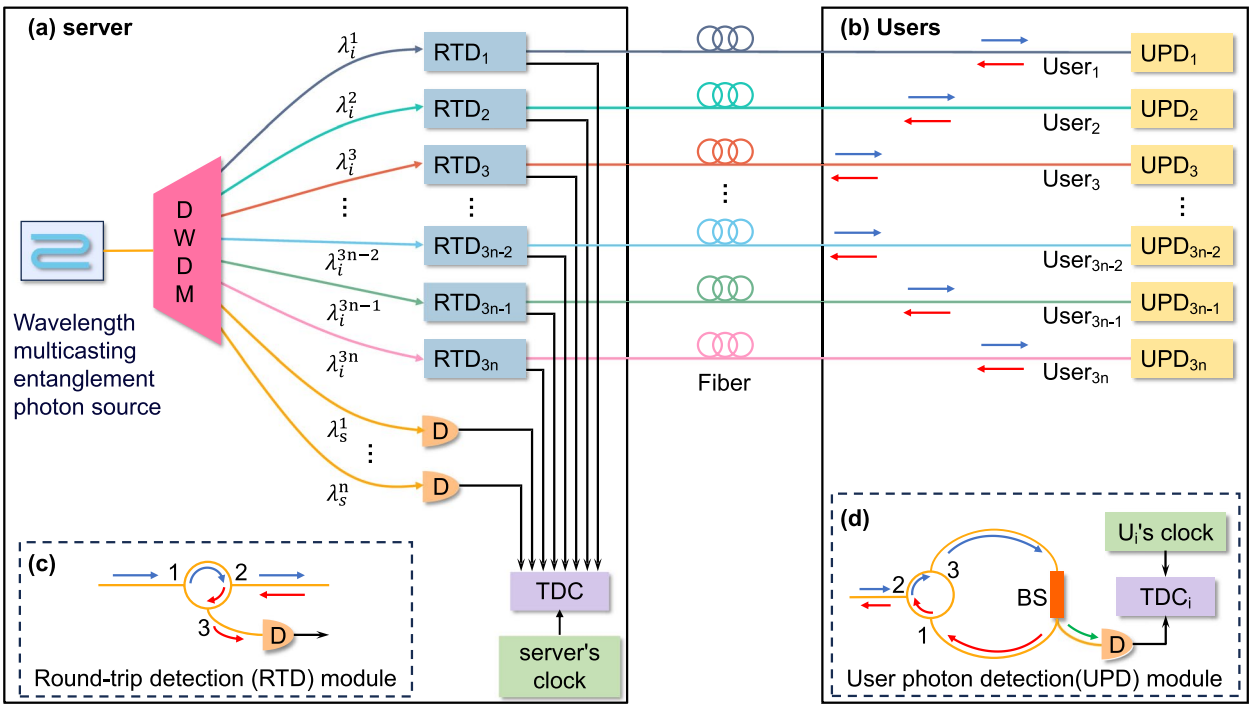

Fig. 2 Schematic diagram of a multi-user round-trip QCS scheme based on wavelength multicasting entanglement photon source. **a** The entangled photon pairs are demultiplexed by DWDM. The idler photons are then transmitted to the user after passing through a round-trip detection (RTD) module. The signal photons are transmitted to a detector for detection. **b** After the photons transmitted from the server to the user enter a user photon detection (UPD) module, the detector detects a portion of the photons, while the other portion returns to the server. **c** RTD module: the input photons pass through an optical circulator (OC) from port 1 to port 2 and the round-trip photons are detected by a detector. **d** UPD module: the input photons pass through an OC (from port 2 to port 3) and a beam splitter (BS), with a portion being detected directly and another portion being sent back to the server through port 1 to port 2 of the OC. The server's and user's detectors are connected to their respective time-to-digital converters (TDC), which are synchronized by their local clocks

time difference τ_{s-u} between t_1 and t_2 consists of Δt_{s-u} (the time needed for the photons to reach User_1 from the server) and the clock difference Δt_1, which can be expressed as

$$\tau_{s-u} = t_2 - t_1 = \Delta t_{s-u} + \Delta t_1 \tag{2}$$

The time difference τ_{s-u-s} between t_1 and t_3 represents the whole round-trip propagation time Δt_{s-u-s} of the photons between the server and User_1, which can be expressed as

$$\tau_{s-u-s} = t_3 - t_1 = \Delta t_{s-u-s} \tag{3}$$

Since the photons have the same round-trip propagation time between the server and User_1, it can be derived that the clock difference is expressed as

$$\Delta t_1 = \tau_{s-u} - \frac{\tau_{s-u-s}}{2} \tag{4}$$

The clock difference Δt_a between other users and the server can also be calculated using the method described above, where $a \in [1, 3n], n \in N^*$. The clock difference between any two users User_a and User_b can be expressed as

$$\Delta t_{a-b} = \Delta t_a - \Delta t_b \tag{5}$$

where $a, b \in [1, 3n], n \in N^*$.

In the network scheme, the number of wavelength channels occupied is $\left\lceil \frac{4m}{3} \right\rceil$ for m users, which can decrease the consumption of wavelength channels by at least 25% compared to the scheme proposed by Tang et al. [15], under the same network scale. Specifically, when equipped with $3m$ users, wavelength channel consumption is decreased by $\frac{1}{3}$. This significant enhancement demonstrates the superiority and potential of our scheme in the QCS network.

4 Experimental setup

In the experiment, we set up a server and three users (Alice, Bob, and Charlie) to demonstrate the wavelength multicasting QCS network, shown in Fig. 3. The pump source is generated by two tunable lasers with center wavelengths of 1555.75 nm and 1544.53 nm, corresponding to International Telecommunication Union's (ITU, 100 GHz) channels C27 and C41, respectively.

Pump lights are amplified by erbium-doped fiber amplifiers (EDFA) respectively. The amplified spontaneous emission (ASE) noise and pump sideband noise are filtered out using a DWDM. Then, the two pump lights are combined into a beam of light by BS_1. A polarization controller (PC) adjusts the pump light for polarization and then pairs it into a silicon waveguide through a grating coupler. At the other end of the waveguide, a

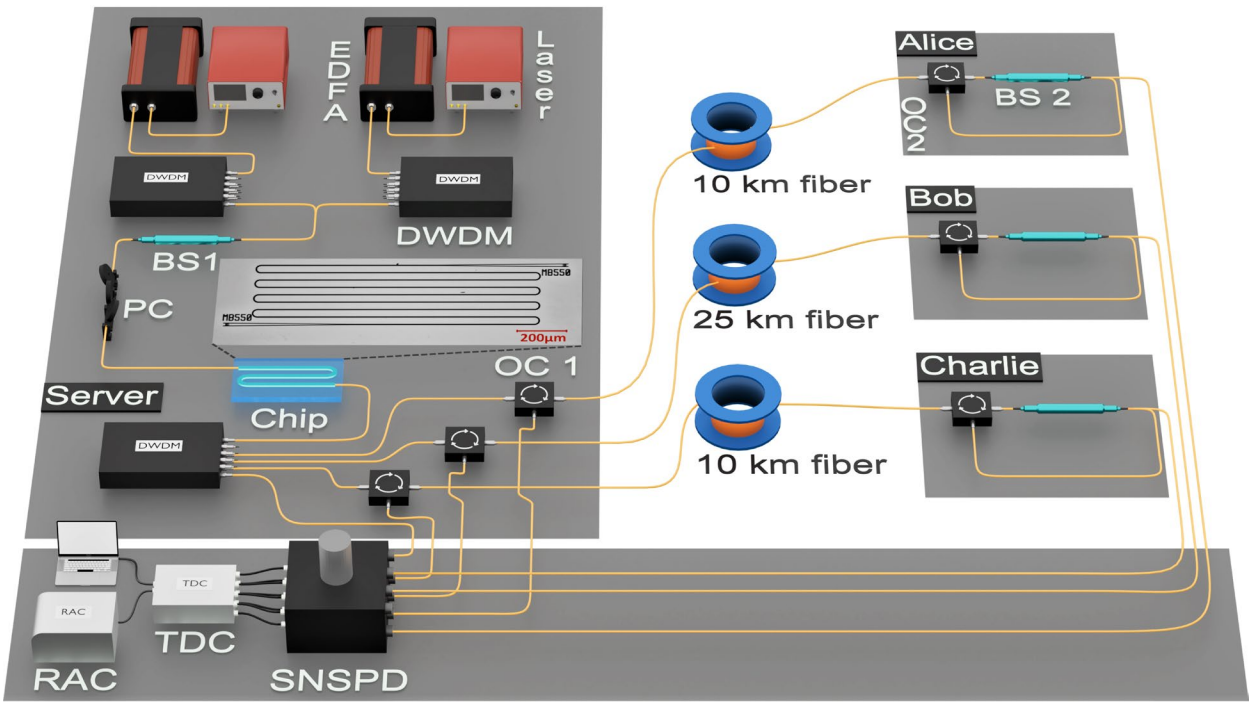

Fig. 3 Experimental setup of round-trip multiple users (one server and three users) QCS based on wavelength multicasting entanglement photon source. EDFA, erbium-doped fiber amplifier; DWDM, dense wavelength division multiplexer; BS, beam splitter; PC, polarization controller; OC, optical circulator; SNSPD, superconducting nanowire single-photon detector; TDC, time-to-digital converters; RAC, rubidium atomic clock

DWDM is connected to filter out the residual pump light and demultiplex the generated signal-idler photon pairs. The signal photons correspond to ITU C33, centered at 1550.92 nm. The idler photons correspond to C21 (centered at 1560.61 nm), C35 (centered at 1549.32 nm), and C49 (centered at 1538.19 nm), respectively. The signal photons are detected by the superconducting nanowire single-photon detector (SNSPD) after exiting from the DWDM and are time-stamped by the TDC. The TDC's clock is synchronized with the location's clock. Alice and Charlie are connected to the server by 10 km fiber through C49 and C21, respectively. Bob is connected to the server by 25 km fiber through C35.

We take the clock synchronization between Alice and the server as an example to describe the experiment. Photons from C49 undergo DWDM demultiplexing and an OC_1 and then travel over fiber of 10 km to OC_2 and BS_2, where they split into two parts. One part is transmitted to Alice for detection. The other part will return to the server by re-enter OC_2 and the fiber of 10 km. The returned photons arrive at the server from port 3 of OC_1 and are detected by the SNSPD. The outputs of SNSPD are connected to a TDC. Furthermore, the rubidium atomic clock (RAC) provides an accurate reference clock for the TDC [36], which serves to reduce the clock drift and jitter of the TDC, thereby enhancing the accuracy of the measurements.

5 Analysis of results

During the experiment, the time differences τ_{s-u} and τ_{s-u-s} were calculated at intervals of 20 s using the Eqs. (2) and (3) to ensure the accuracy of the results. The Gaussian fitting results for the first 20 s are shown in Fig. 4.

Due to the presence of group velocity dispersion in optical fibers, the full width at half maximum (FWHM) of $G^{(2)}(\tau_{s-u-s})$ coincidence histogram belonging to Bob is greater than the FWHM of $G^{(2)}(\tau_{s-u})$. However, Alice and Charlie exhibit completely different phenomena from those mentioned above. This is due to the different noise levels in the channels used by the users, leading to different photon counts. An increase in photon count

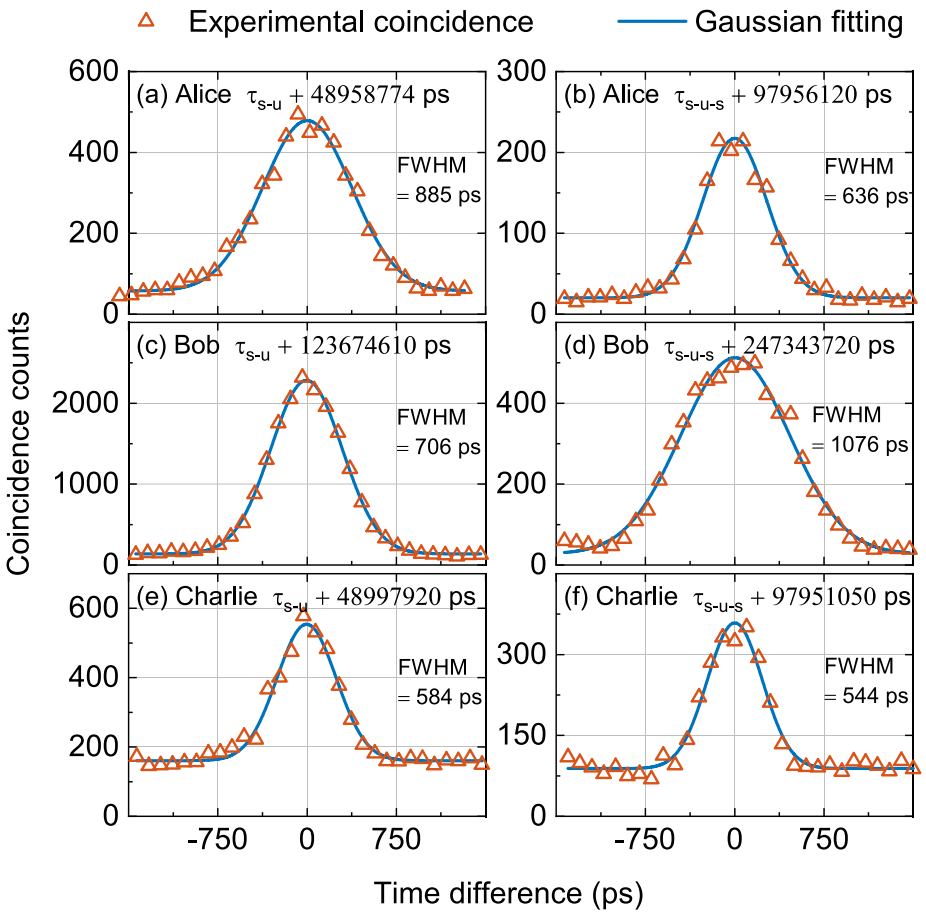

Fig. 4 The coincidence count histograms of $G^{(2)}(\tau_{s-u})$ and $G^{(2)}(\tau_{s-u-s})$ in the first 20 s experiment. **a** and **b** show the coincidence histograms $G^{(2)}(\tau_{s-u})$ and $G^{(2)}(\tau_{s-u-s})$ of Alice, while (**c** and **d**) as well as (**e** and **f**) show the same for Bob and Charlie, respectively

exacerbates the time drift in SNSPD [37] and affects the extreme points and full width at FWHM of the coincidence counting histogram. The time differences τ_{s-u} and τ_{s-u-s} between the server and the users over consecutive 11.1 hours are shown in Fig. 5. The time differences τ_{s-u} and τ_{s-u-s} for each user are calculated from the fitting results. The τ_{s-u} (τ_{s-u-s}) expectations between the server and each user (Alice, Bob, and Charlie) are −48959057 ps (−97956545 ps), −123674816 ps (−247344032 ps), and −48998153 ps (−97951379 ps), respectively.

The fluctuations for Bob are less pronounced than those for other users within the same time, mainly due to two reasons: firstly, the degree of time drift of the SNSPD varies among them. Secondly, Bob's Coincidences-to-Accidentals Ratio (CAR) is significantly higher than other users, contributing to more accurate and stable results during the Gaussian fitting process. Overall, time difference measurements are affected by noise. Furthermore, because of the intrinsic instability of the chip coupling platform, manual adjustments of the coupling efficiency may occasionally be required during the experiment to ensure the stability of the number of photon pairs generated. This results in a sudden change in the photon count for each channel, leading to abrupt variations in the time differences τ_{s-u} and τ_{s-u-s} (the extreme points of the Gaussian fitting of the coincidence count histogram), as illustrated in the Fig. 5. However, the variation in τ_{s-u-s} for each user is about twice the variation in τ_{s-u}. Therefore, these variations tend to offset each other when calculating the clock difference.

The clock difference Δt can be calculated according to Eq. (4), as shown in Fig. 6. The standard deviations of the clock difference between the server and each user (Alice, Bob, and Charlie) are 16.2006 ps, 6.2810 ps, and 14.6764 ps, respectively. The non-zero value of Δt can be attributed to the transmission time asymmetry of various system components (such as BS, OC, DWDM, and PC) and the time drift of the SNSPD [15].

Figure 7 demonstrates the TDEV between the server and each user (Alice, Bob, and Charlie), which at an average time of 640 s is 3.43 ps, 2.03 ps, and 2.44 ps, respectively. The TDEV of Bob is superior to those of Alice and Charlie. Initially, the noise level of the wavelength channel utilized by Bob was lower than that of the other two

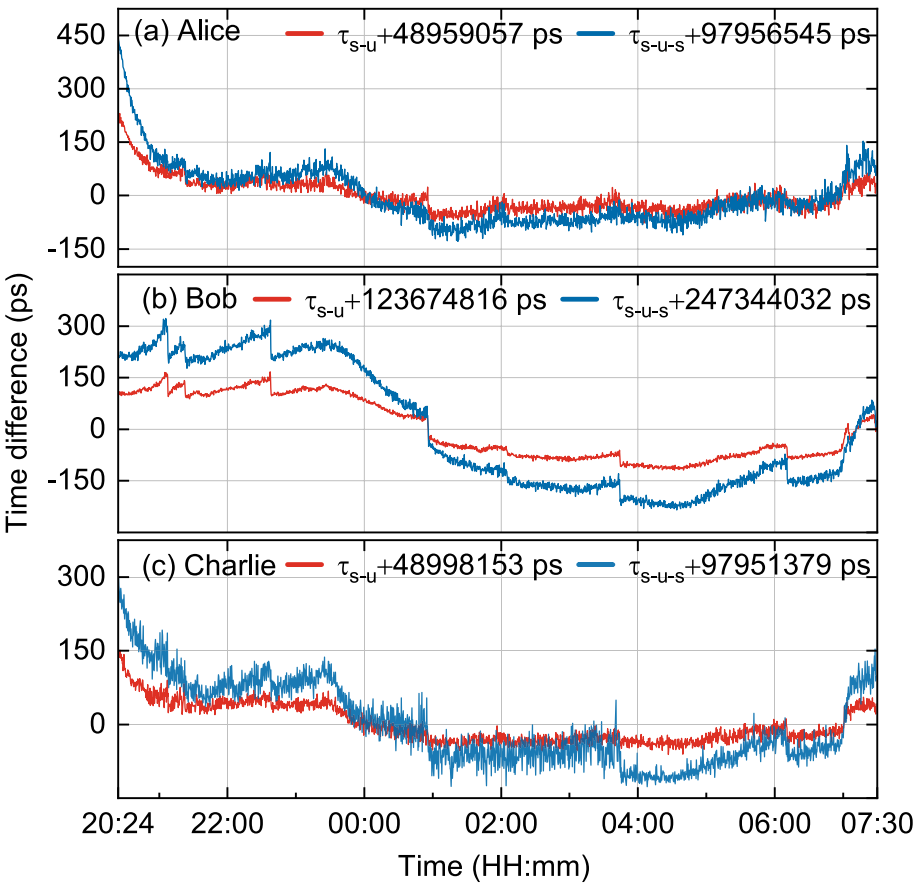

Fig. 5 The measured time differences between each user and the server at intervals of 20 s

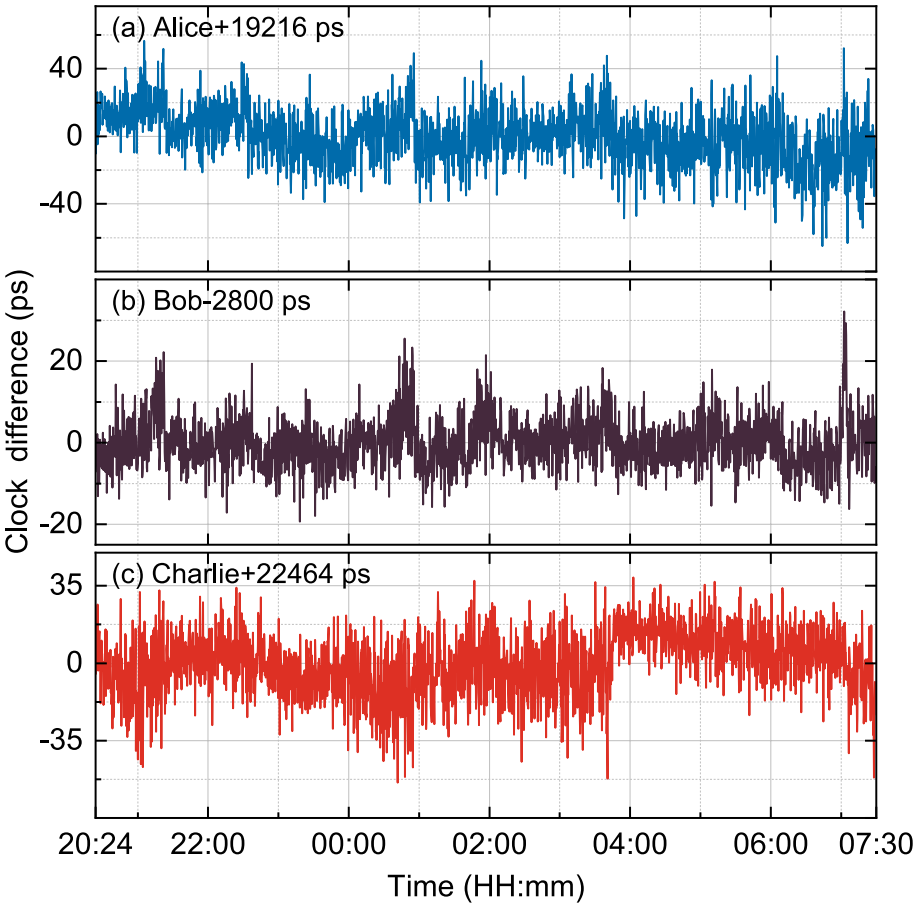

Fig. 6 The clock differences between each user and the server measured in the experiment

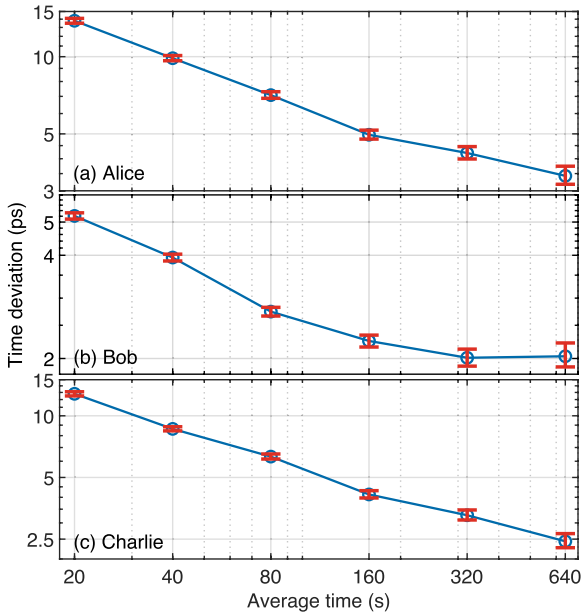

Fig. 7 The TDEV of the measured clock differences by each user in the experiment

users. Different noise levels lead to variations in both the CAR and photon count, resulting in more stable and accurate Gaussian fitting results. A stable and precise Gaussian fitting indicates a stable time difference, which in turn reduces fluctuations in the clock difference. Ultimately, smaller fluctuations in clock difference lead to a smaller TDEV calculation result. In conclusion, to achieve a lower TDEV, it is necessary to reduce the noise level and maintain an appropriate photon count, which can improve performance even over longer transmission distances.

6 Conclusion

In this paper, we propose a more efficient QCS network scheme with the wavelength multicasting entangled photon source, which can decrease at least 25% of wavelength channel consumption compared with the previous QCS network scheme under the same network scale. Afterwards, the four node QCS network is demonstrated, where the wavelength multicasting entangled photon source utilize with dual-pumped FWM silicon chip. The demonstration lasted for 11.1 h. The fiber of 10 km connection is between

the Alice and Charlie server, and 25 km fiber connection is between Bob and server. The time deviation (TDEV) between the server and each user (Alice, Bob, and Charlie) at an average time of 640 s is 3.43 ps, 2.03 ps, and 2.44 ps respectively. In addition, the scale of wavelength multicasting can be expanded by adding pump lights of different wavelengths, so that one signal wavelength channel can be entangled with more idle optical wavelength channels, which further decreases the consumption of wavelength channel and flexibly adapts to more complex network environments. When the number of users is an integer multiple of the number of idler wavelength channels entangled with a signal wavelength channel, the wavelength channel saving will be maximized. Our scheme is expected to play a key role in future quantum networks, laying the foundation for achieving larger-scale QCS networks.

Acknowledgements
Not applicable.

Authors' contributions
H.C. and B.L. proposed the scheme. J.A.L. and H.H. designed performed the experiment, and contributed equally. This work was supervised by H.C., B.L., and Z.K.L., and co-supervised by Z.J.Z. and J.B.Y. G.K. designed the chip. X.P.H., B.Y.T., J.Q.H., S.Y.X., and W.R.Y. contributed to the data collection and analysis. J.A.L. and H.H. wrote the draft and all authors reviewed the manuscript.

Funding
This research was funded by the National Key R&D Program of China (2022YFF0706005); National Natural Science Foundation of China (62275271,62305387); Foundation of NUDT (ZK23-03); Hunan Provincial Natural Science Foundation of China (2022JJ40552,2023JJ40683); State Key Laboratory of High Performance Computing, NUDT (202201-12); Science and Technology Innovation Program of Hunan Province (2023RC3003); and Guangxi Science and Technology Major Project (GuikeAA23073013).

Data availability
Experimental data is made available upon request by the corresponding author.

Declarations

Competing interests
The authors declare that they have no competing interests.

Received: 13 September 2024 Accepted: 21 October 2024
Published online: 18 November 2024

References

1. H. Esteban, J. Palacio, F.J. Galindo, T. Feldmann, A. Bauch, D. Piester, Improved gps-based time link calibration involving roa and ptb. IEEE T Ultrason FERR. **57**(3), 714–720 (2010). https://doi.org/10.1109/TUFFC.2010.1469
2. P. Exertier, A. Belli, E. Samain, W. Meng, H. Zhang, K. Tang, A. Schlicht, U. Schreiber, U. Hugentobler, I. Procházka et al., Time and laser ranging: a window of opportunity for geodesy, navigation, and metrology. J. Geod. **93**, 2389–2404 (2019). https://doi.org/10.1007/s00190-018-1173-8
3. S.W. Schediwy, D.R. Gozzard, C. Gravestock, S. Stobie, R. Whitaker, J.A. Malan, P. Boven, K. Grainge, The mid-frequency square kilometre array phase synchronisation system. Publ. Astron. Soc. Aust. **36**, e007 (2019). https://doi.org/10.1017/pasa.2018.48
4. C. Clivati, R. Aiello, G. Bianco, C. Bortolotti, P.D. Natale, V.D. Sarno, P. Maddaloni, G. Maccaferri, A. Mura, M. Negusini, F. Levi, F. Perini, R. Ricci, M. Roma, L.S. Amato, M.S. de Cumis, M. Stagni, A. Tuozzi, D. Calonico, Common-clock very long baseline interferometry using a coherent optical fiber link. Optica **7**(8), 1031–1037 (2020). https://doi.org/10.1364/OPTICA.393356
5. M. Wang, F. Zhang, Squeezing for cosmic symphony. AAPPS Bull. **33**(1), 5 (2023). https://doi.org/10.1007/s43673-023-00076-5
6. A. Mahmood, M.I. Ashraf, M. Gidlund, J. Torsner, J. Sachs, Time synchronization in 5g wireless edge: Requirements and solutions for critical-mtc. IEEE Commun. Mag. **57**(12), 45–51 (2019). https://doi.org/10.1109/MCOM.001.1900379
7. L. Sliwczynski, P. Krehlik, H. Imlau, H. Ender, H. Schnatz, D. Piester, A. Bauch, Fiber-based utc dissemination supporting 5g telecommunications networks. IEEE Commun. Mag. **58**(4), 67–73 (2020). https://doi.org/10.1109/MCOM.001.1900599
8. D. Pan, X.T. Song, G.L. Long, Free-space quantum secure direct communication: Basics, progress, and outlook. Adv. Devices Instrum. **4**, 0004 (2023). https://doi.org/10.34133/adi.0004
9. J. Zhang, F. Zhu, Z. Yang, C. Chen, X. Tian, X. Guan, Routing and scheduling co-design for holistic software-defined deterministic network. Fundam. Res. **4**(1), 25–34 (2024). https://doi.org/10.1016/j.fmre.2023.11.007
10. F. Hou, R. Quan, R. Dong, X. Xiang, B. Li, T. Liu, X. Yang, H. Li, L. You, Z. Wang, S. Zhang, Fiber-optic two-way quantum time transfer with frequency-entangled pulses. Phys. Rev. A. **100**, 023849 (2019). https://doi.org/10.1103/PhysRevA.100.023849
11. R. Quan, H. Hong, W. Xue, H. Quan, W. Zhao, X. Xiang, Y. Liu, M. Cao, T. Liu, S. Zhang, R. Dong, Implementation of field two-way quantum synchronization of distant clocks across a 7 km deployed fiber link. Opt. Express **30**(7), 10269–10279 (2022). https://doi.org/10.1364/OE.451172
12. H. Hong, R. Quan, X. Xiang, W. Xue, H. Quan, W. Zhao, Y. Liu, M. Cao, T. Liu, S. Zhang, R. Dong, Demonstration of 50 km fiber-optic two-way quantum clock synchronization. J. Lightwave Technol. **40**(12), 3723–3728 (2022). https://doi.org/10.1109/JLT.2022.3153655
13. H. Hong, R. Quan, X. Xiang, Y. Liu, T. Liu, M. Cao, R. Dong, S. Zhang, Quantum two-way time transfer over a 103 km urban fiber. J. Lightw. Technol. (2023). https://doi.org/10.1109/JLT.2023.3323434
14. R. Quan, R. Dong, Y. Zhai, F. Hou, X. Xiang, H. Zhou, C. Lv, Z. Wang, L. You, T. Liu, S. Zhang, Simulation and realization of a second-order quantum-interference-based quantum clock synchronization at the femtosecond level. Opt. Lett. **44**(3), 614–617 (2019). https://doi.org/10.1364/OL.44.000614
15. Y. Tang Bang, M. Tian, H. Chen, H. Han, H. Zhou, S. Li, B. Xu, R. Dong, B. Liu, W. Yu, Demonstration of 75 km-fiber quantum clock synchronization in quantum entanglement distribution network. EPJ Quantum Technol. **10**(1), 50 (2023). https://doi.org/10.1140/epjqt/s40507-023-00207-9
16. J. Lee, L. Shen, A.N. Utama, C. Kurtsiefer, Absolute clock synchronization with a single time-correlated photon pair source over a 10 km optical fibre. Opt. Express **30**(11), 18530–18538 (2022). https://doi.org/10.1364/OE.455542
17. U.A. Javid, J. Ling, J. Staffa, M. Li, Y. He, Q. Lin, Ultrabroadband entangled photons on a nanophotonic chip. Phys. Rev. Lett. **127**(18), 183601 (2021). https://doi.org/10.1103/PhysRevLett.127.183601
18. K. Guo, J. Feng, X. Shi, J. Li, M. Gao, H. Jing, X. Wang, J. Yang, H. Ou, Experimentally validated full-vectorial model of wavelength multicasting via four-wave mixing in straight waveguides. Sci. Rep. **8**(1), 13030 (2018). https://doi.org/10.1038/s41598-018-31470-x
19. X. Wang, L. Huang, S. Gao, Low-power-penalty wavelength multicasting for 36 gbit/s 16-qam coherent optical signals in a silicon waveguide. Opt. Lett. **39**(24), 6907–6910 (2014). https://doi.org/10.1364/OL.39.006907
20. W. Wen, Z. Chen, L. Lu, W. Yan, W. Xue, P. Zhang, Y. Lu, S. Zhu, X.S. Ma, Realizing an entanglement-based multiuser quantum network with integrated photonics. Phys. Rev. Appl. **18**, 024059 (2022). https://doi.org/10.1103/PhysRevApplied.18.024059
21. B. Lu, L. Liu, J.Y. Song, K. Wen, C. Wang, Recent progress on coherent computation based on quantum squeezing. AAPPS Bull. **33**(1), 7 (2023). https://doi.org/10.1007/s43673-023-00077-4
22. A.S. Dellios, M.D. Reid, P.D. Drummond, Simulating gaussian boson sampling quantum computers. AAPPS Bull. **33**(1), 31 (2023). https://doi.org/10.1007/s43673-023-00099-y
23. L. Feng, G. Guo, X. Ren, Progress on integrated quantum photonic sources with silicon. Adv. Quantum Technol. **3**(2), 1900058 (2020). https://doi.org/10.1002/qute.201900058

24. Y. Li, Z. Zhou, L. Feng, W. Fang, S. Liu, S. Liu, K. Wang, X. Ren, D. Ding, L. Xu et al., On-chip multiplexed multiple entanglement sources in a single silicon nanowire. Phys. Rev. Appl. **7**(6), 064005 (2017). https://doi.org/10.1103/PhysRevApplied.7.064005
25. I.B. Djordjevic, On global quantum communication networking. Entropy **22**(8) (2020). https://doi.org/10.3390/e22080831
26. L. Caspani, C. Reimer, M. Kues, P. Roztocki, M. Clerici, B. Wetzel, Y. Jestin, M. Ferrera, M. Peccianti, A. Pasquazi et al., Multifrequency sources of quantum correlated photon pairs on-chip: a path toward integrated quantum frequency combs. Nanophotonics **5**(2), 351–362 (2016). https://doi.org/10.1515/nanoph-2016-0029
27. J.W. Silverstone, D. Bonneau, K. Ohira, N. Suzuki, H. Yoshida, N. Iizuka, M. Ezaki, C.M. Natarajan, M.G. Tanner, R.H. Hadfield et al., On-chip quantum interference between silicon photon-pair sources. Nat. Photon. **8**(2), 104–108 (2014). https://doi.org/10.1038/nphoton.2013.339
28. X. Lu, Q. Li, D.A. Westly, G. Moille, A. Singh, V. Anant, K. Srinivasan, Chip-integrated visible-telecom entangled photon pair source for quantum communication. Nat. Phys. **15**(4), 373–381 (2019). https://doi.org/10.1038/s41567-018-0394-3
29. K. Inoue, H. Toba, Wavelength conversion experiment using fiber four-wave mixing. IEEE Photon. Technol. Lett. **4**(1), 69–72 (1992). https://doi.org/10.1109/68.124880
30. W. Wang, L. Rau, D. Blumenthal, 160 gb/s variable length packet/10 gb/s-label all-optical label switching with wavelength conversion and unicast/multicast operation. J. Lightwave Technol. **23**(1), 211–218 (2005). https://doi.org/10.1109/JLT.2004.840044
31. M. Zhang, L. Feng, Z. Zhou, Y. Chen, H. Wu, M. Li, S. Gao, G. Guo, G. Guo, D. Dai et al., Generation of multiphoton quantum states on silicon. Light Sci. Appl. **8**(1), 41 (2019). https://doi.org/10.1038/s41377-019-0153-y
32. S. Dong, Q. Zhou, W. Zhang, Y. He, W. Zhang, L. You, Y. Huang, J. Peng, Energy-time entanglement generation in optical fibers under cw pumping. Opt. Express **22**(1), 359–368 (2014). https://doi.org/10.1364/OE.22.000359
33. H. Takesue, K. Inoue, Generation of 1.5$-\mu$m band time-bin entanglement using spontaneous fiber four-wave mixing and planar light-wave circuit interferometers. Phys. Rev. A **72**, 041804 (2005). https://doi.org/10.1103/PhysRevA.72.041804
34. R. Quan, R. Dong, X. Xiang, B. Li, T. Liu, S. Zhang, High-precision nonlocal temporal correlation identification of entangled photon pairs for quantum clock synchronization. Rev. Sci. Instrum. **91**(12) (2020). https://doi.org/10.1063/5.0031166
35. R.J. Glauber, The quantum theory of optical coherence. Phys. Rev. **130**, 2529–2539 (1963). https://doi.org/10.1103/PhysRev.130.2529
36. J. Zhang, T. Shi, J. Miao, J. Chen, The development of active optical clock. AAPPS Bull. **33**(1), 10 (2023). https://doi.org/10.1007/s43673-023-00079-2
37. A. Mueller, E.E. Wollman, B. Korzh, A.D. Beyer, L. Narvaez, R. Rogalin, M. Spiropulu, M.D. Shaw, Time-walk and jitter correction in snspds at high count rates. Appl. Phys. Lett. **122**(4) (2023). https://doi.org/10.1063/5.0129147

Publisher's Note